Supplement of Clim. Past, 18, 559–577, 2022
https://doi.org/10.5194/cp-18-559-2022-supplement

Supplement of

Biomarker proxy records of Arctic climate change during the Mid-Pleistocene transition from Lake El'gygytgyn (Far East Russia)

Kurt R. Lindberg et al.

Correspondence to: Kurt R. Lindberg (kurtlind@buffalo.edu)

1 Introduction

This supplement contains Figures S1-S9 and associated discussion.

1.1 Leaf wax *n*-alkane distributions

The apolar fractions of the Lake El'gygytgyn lipid extracts contained *n*-alkanes with an average total concentration of 6.5 µg g sed^{-1} (n=149) and a high odd/even chain length ratio (Fig. S1). The Carbon Preference Index (Eq. S1) averages 3.6 (± 0.6 SD), indicating that the *n*-alkanes are sourced from plants and are not severely impacted by bacterial degradation.

Eq. S1. $CPI = \left[\frac{\Sigma(C25-C33)_{odd}}{\Sigma(C24-C32)_{even}} + \frac{\Sigma(C25-C33)_{odd}}{\Sigma(C26-C34)_{even}}\right] * 0.5$ (Bray and Evans, 1961)

We observe a shift in the *n*-alkane average chain length through the mid-Pleistocene transition. In order to identify when this transition occurred, we applied the ramp-fitting code published by Capron et al. (2021). Using this approach, we find that the ACL shifted toward higher values between 1019 and 895 ka (95% Confidence Interval), with the transition midpoint at around 946 ka (Fig. S2).

This shift toward higher ACL values coincides with changes in the landscape openness index, which is based on the Lake El'gygytgyn pollen record across the MPT (Zhao et al., 2018). Previously, Zhao et al. (2018) suggest that the Landscape openness index showed a marked change circa 890 ka, in close agreement with, but slightly lagging, the change-point analysis of *n*-alkane ACL values. We investigate the relationship between the pollen-based and the biomarker-based vegetation change through linear regression of these metrics. We resampled the *n*-alkane ACL data to intervals where pollen data were analysed (Fig. S3a), and find a statistically significant, negative correlation with landscape openness, indicating that leaf waxes are in part reflecting changing vegetation assemblages (Fig. S3b, r^2=17, $p<0.001$).

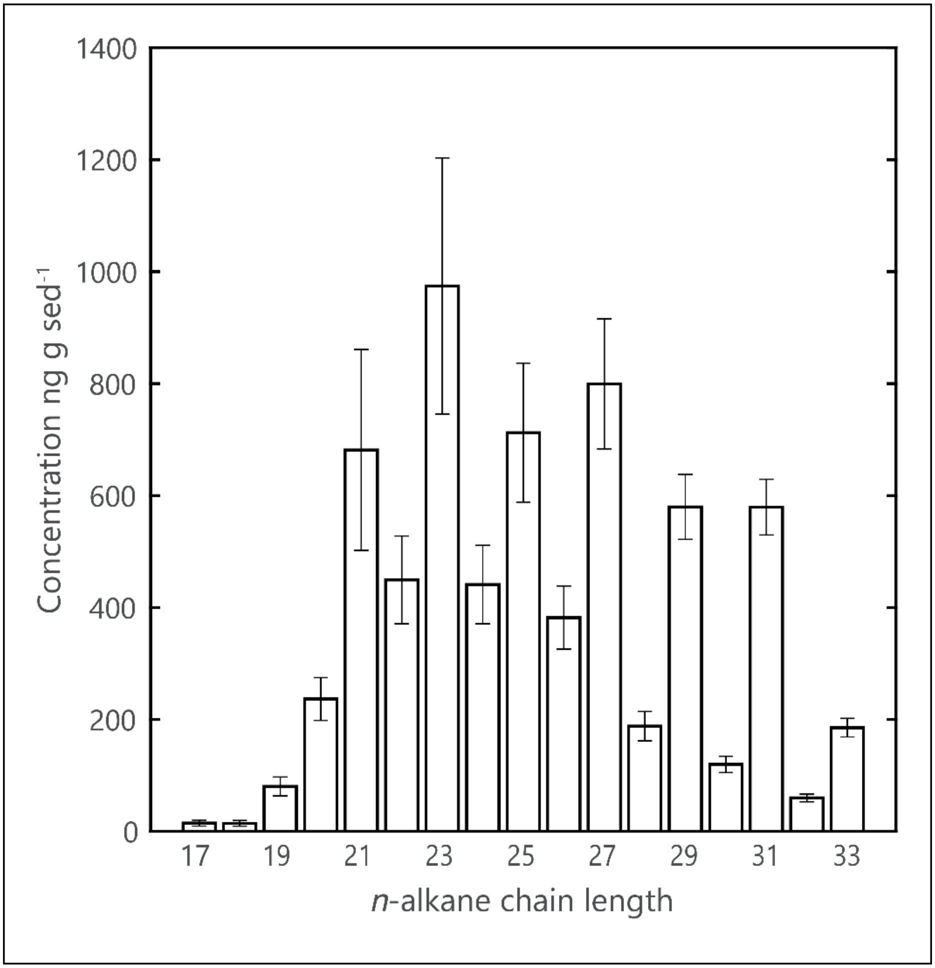

Figure S1: Bar plots of average leaf wax (*n*-alkane) concentrations in Lake El'gygytgyn samples from the MPT. Error bars represent the standard error of the mean (n = 149).

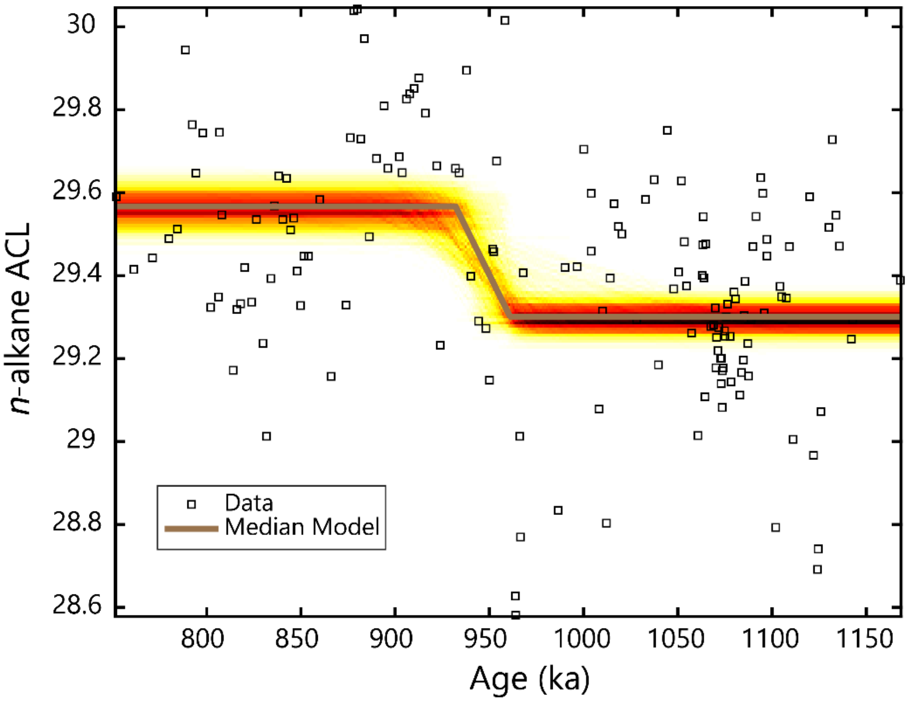

Figure S2: Ramp-fitting analysis of *n*-alkane ACL to statistically identify the transition period of leaf wax distributions.

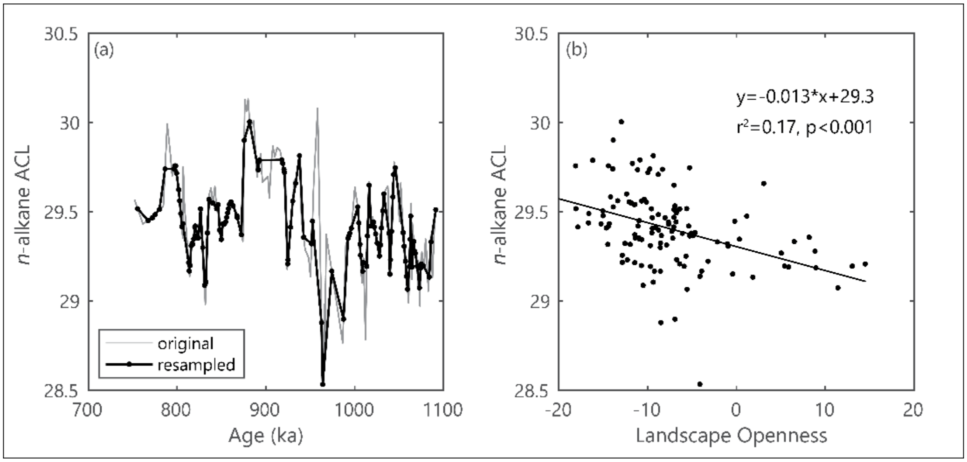

Figure S3: Comparison between leaf wax *n*-alkane average chain length and the pollen-derived landscape openness index (Zhao et al., 2018). A) *n*-alkane ACL after re-sampling to the ages of the pollen data. B) Linear regression between the two variables, showing a negative correlation.

1.2 brGDGTs

In the Lake El'gygytgyn samples analyzed for this study, brGDGT IIIa is the most abundant, followed by the other acyclic compounds IIa and Ia (Fig. S4). As discussed in the main text, hexamethyl compounds are more abundant than pentamethyl or tetramethyl compounds. The ternary diagram (Fig. S5) illustrates how these samples compare to the global calibration samples. There is a strong contrast between the Lake El'gygytgyn samples and the global soil/peat samples of Naafs et al. (2017), which show a predominance of tetramethyl compounds. Siberian soils brGDGT distributions follow the same trend in ternary space as the global soil and peat dataset (Kusch et al., 2019), and have relatively higher abundance of pentamethylated brGDGTs (43 ± 5%) than what we observe in the El’gygytgyn sediments (30 ± 4%). This is a strong indicator that the brGDGTs are sourced from within-lake production rather than from surrounding soils. The lakes calibration (Martínez-Sosa et al., 2021) has a large range in ternary space, with warmer samples represented by tetramethyl-dominant brGDGT distributions. The Lake El’gygytgyn data fall near the upper range of these samples, among other cold climate sites, and show some scatter from the main trend.

The analytical methodology employed here allows for separation of the brGDGT isomers. We find that the relative proportion of 6-methyl brGDGTs ranges from 0.1% to 33%, and averages 9% (Fig. S6). Over the study interval, there is no apparent trend in the percentage of 6-methyl isomers. Weber et al. (2018) previously suggested that in lakes, the proportion of 6-methyl isomers is related to distinct GDGT producers residing in anoxic versus oxic strata depths of the water column. At Lake El’gygytgyn, there is geochemical evidence, based on the Mn/Fe ratio, indicating lake oxygenation has changed during the study interval, possibly impacting the assemblage of brGDGT producers. As such, we prefer to utilize the isomer specific MBT'_{5ME} index for the MPT temperature reconstruction, as it may relate to a narrower group of producers than indices incorporating 5-methyl and 6-methyl isomers. Furthermore, some samples do not contain any 6-methyl isomers and thus MBT'_{5ME} is needed to provide a continuous record.

de Wet et al. (2016) previously analysed brGDGT distributions from MIS 33 to MIS 30 using an HPLC methodology following (Weijers et al., 2007) that did not separate out the 5- and 6-methyl brGDGT isomers. To assess how the updated chromatography affects our results, we compare the subset of samples that were run using both methods. The fractional abundance of IIIa from the de Wet et al. (2016) analyses is tightly correlated with the summed IIIa+IIIa′abundances measured here (Fig. S7a), with the majority of samples falling very near the 1:1 line. The same is true for IIa (old method) and IIa+IIa′ (new method, Fig. S7b). This differs somewhat from the results of Russell et al. (2018), who found, in a comparison between methods, that most data points fell off of the 1:1 line, which they attribute to the way the partially-separated peaks were integrated using the old method. With low 6-methyl isomers present, this problem is not as apparent in our Lake El’gygytgyn dataset. We further compare the MBT'_{5ME} values with the MBT′ values calculated from de Wet’s data. Again, we find a very tight correlation, but observe that the MBT'_{5ME} values tend fall below the 1:1 line, particularly at the low range of MBT′ values

(Fig. S7c). Lastly, comparing the BayMBT temperatures derived from the isomer-specific analysis with the original temperatures reported from de Wet et al. (2016), we find that the temperatures are well-correlated, but with a slope of approximately 0.5 (Fig. S7d). That is, the temperature variability reconstructed for Months Above Freezing using BayMBT is roughly half the amplitude previously reconstructed for Mean Annual Air Temperature.

Comparing the recent calibrations, all of which separate the 5- and 6-methyl isomers, we find that the magnitude of temperature variability as well as the absolute values vary between calibrations (Fig. S8). Reconstructed temperatures using the African lakes calibration (Russell et al., 2018) range from 2.2 to 17.0 ºC, with a mean of 7.8 ºC. Temperatures based on the Greenland calibration (Zhao et al., 2021) range from 4.0 to 29.7 °C, with a mean of 13.6 °C. The lacustrine BayMBT calibration (Martínez-Sosa et al., 2021) yields median values ranging from 2.8 to 15.7 °C, with a mean of 7.1 °C. Two of the calibrations from Raberg et al. (2021) applied here yield ranges of -1.9 to 18.7 °C (mean 9.1 °C) for the "full" calibration and 1.0 to 16.2 °C (mean 7.3 °C) for the "meth" calibration. Results from the Feng et al. (2019) calibration, which is calibrated to MAAT, range from -27.9 to 5.3 °C, with a mean of -9.9 ·C.

Figure S8 shows the raw MBT'_{5ME} data, along with the six lakes-based calibrations discussed in the main text (Dang et al., 2018; Russell et al., 2018; Feng et al., 2019; Martínez-Sosa et al., 2021; Zhao et al., 2021; Raberg et al., 2021). Naturally, the temporal structure of the reconstructions is identical for the three reconstructions based on the MBT'_{5ME} index (Fig. S8b-d). The most significant difference observed is the much higher magnitude of variability in the application of the Greenland Lake *in-situ* calibration of Zhao et al. (2021). The temperature reconstructions resulting from the calibration of Raberg et al. (2021) differ dramatically whether the full suite or the partial suite of brGDGTs is used (Fig. S8e-f). Using the full set, we see many similarities with the MBT'_{5ME} results, such as strong warming during MIS 21 and 29, and moderate warming during MIS 31. Using just the "Meth" set, the resulting reconstruction disagrees with several other reconsructions. For example, the warming during MIS 31 is lower-magnitude than other reconstructions, either based on brGDGTs or on pollen. Likewise, warming during MIS 21 is apparent in the MBT'_{5ME} and in the pollen record, but absent from the "Meth" calibration.

Figure S9 illustrates the relationship between the Lake El'gygytgyn MBT'_{5ME} record and orbital parameters during the MPT. In Fig. S9a, we observe that the temperature reconstruction tends to track the 41 kyr obliquity cycle, particularly in the older part of the interval. In Fig. S9b, we observe that summer insolation, dominantly controlled by the precession parameter, tracks many of the higher-frequency temperature changes. Notably, the terminations of MIS 32, 30, and 22 see increases in both the Earth's tilt and the summer insolation. Some divergences between the temperature reconstruction and orbital variations are also evident. Most notably are the brief cold interval during MIS 23 which aligns with maxima in insolation and obliquity, and the return to glacial conditions during the upper portion of MIS 21 which also aligns with maxima in the orbital parameters.

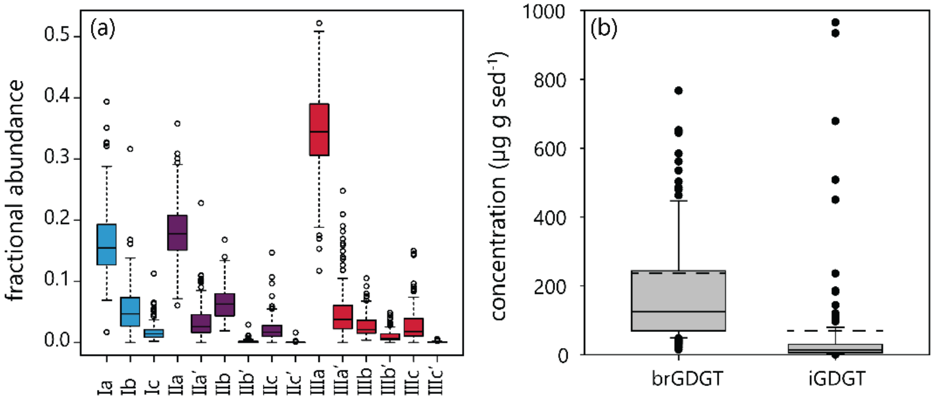

Figure S4: A) Boxplots of average brGDGT distributions in Lake El'gygytgyn samples from the MPT. Tetramethylated brGDGTs are shown in blue, pentamethylated brGDGTs in purple, and hexamethylated brGDGTs in red. The dominance of the 5-methyl isomers over the 6-methyl isomers (the brGDGT numbers Roman numerals and letters denoted with a prime symbol) is clear. B) Boxplots showing average concentrations of branched and isoprenoid GDGTs; brGDGT dominate Lake El'gygytgyn sediments. The solid line indicates the median value and the dashed line the mean. Two brGDGT outliers at 4213 and 4561 µg g sed^{-1} lie outside the scale of the Y-axis and therefore are not shown; nor is one iGDGT outlier at 3917 µg g sed^{-1}.

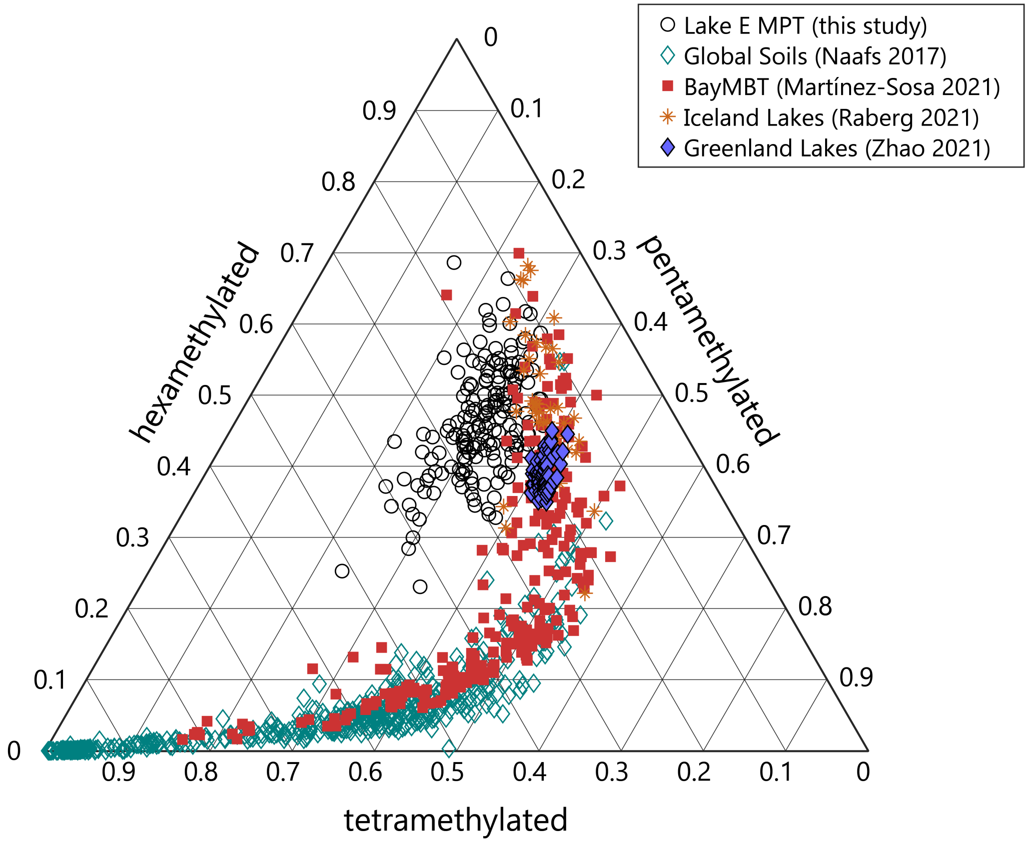

Figure S5: Ternary diagram showing the relative abundance of tetra-, penta-, and hexa-methylated brGDGTs in the Lake El'gygytgyn study interval (open black circles), and previously published calibration datasets including the BayMBT lakes dataset (Martínez-Sosa et al., 2021), the global soils dataset of Naafs et al. (2017), Icelandic lakes from Raberg et al. (2021) and Lake 578 in Greenland (Zhao et al., 2021).

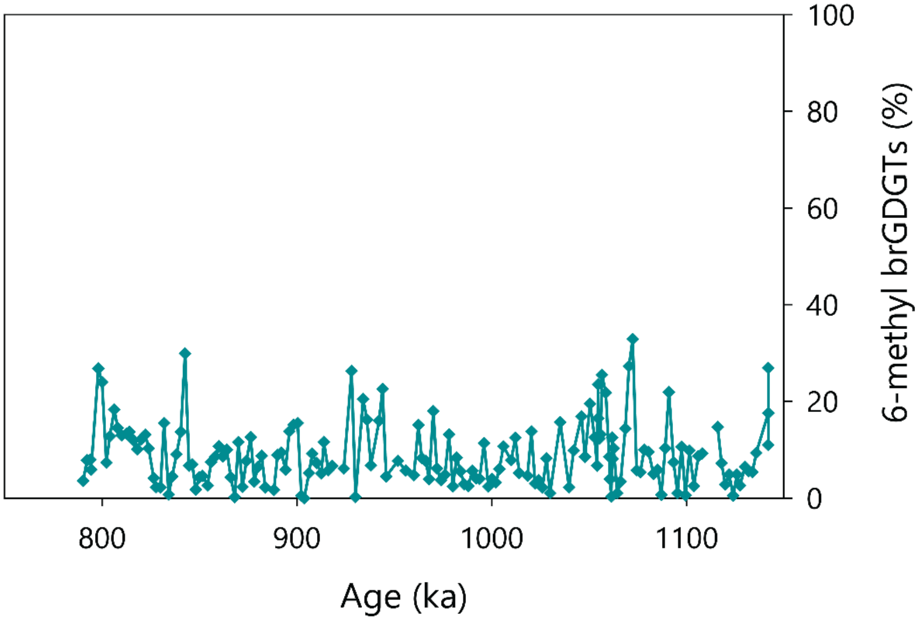

Figure S6: Total percent of 6-methyl brGDGTs at Lake El'gygytgyn during the MPT.

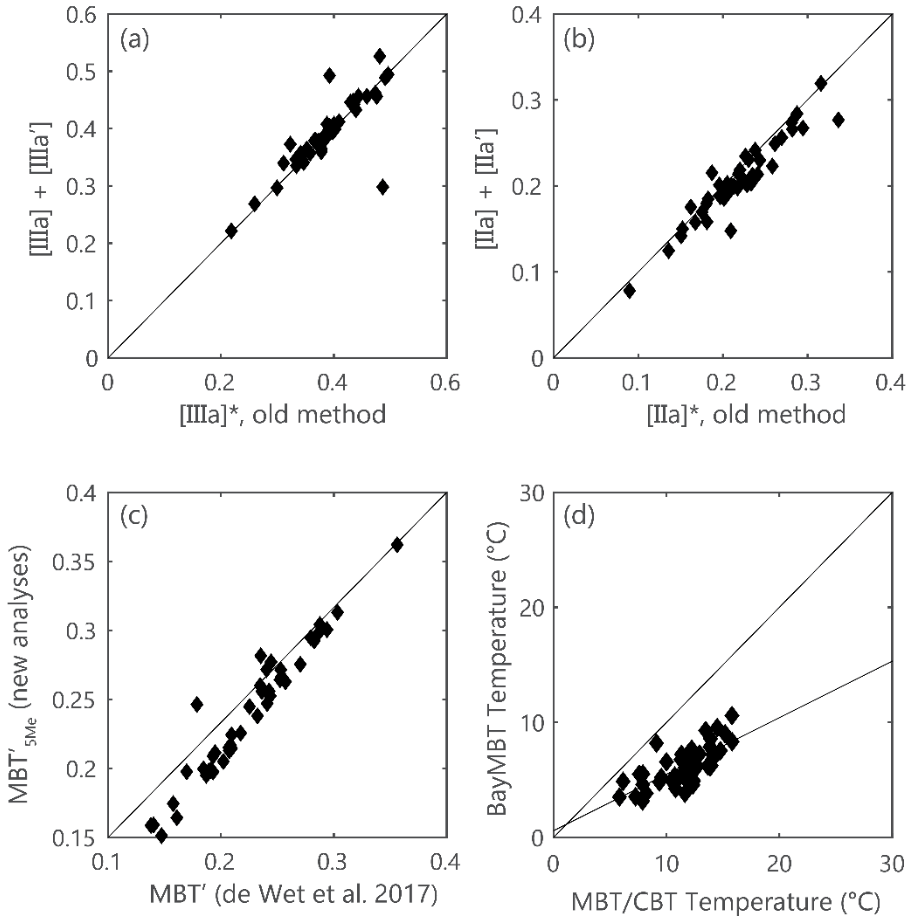

Figure S7: Comparison of brGDGT results and temperature inferences between samples analyzed on the Prevail Cyano HPLC column (old-method) (de Wet et al., 2016; Hopmans et al., 2000) and reanalyzed in this study using the BEH-HILIC columns following Hopmans et al. (2016). A) fractional abundance of [IIIa+IIIa'] versus [IIIa-old method]. B) fractional abundance of [IIa+IIa'] versus [IIa-old method]. C) MBT' (5-methyl only) versus MBT' (old method). D) BayMBT-derived temperature versus MBT/CBT temperatures reported by de Wet et al. (2016).

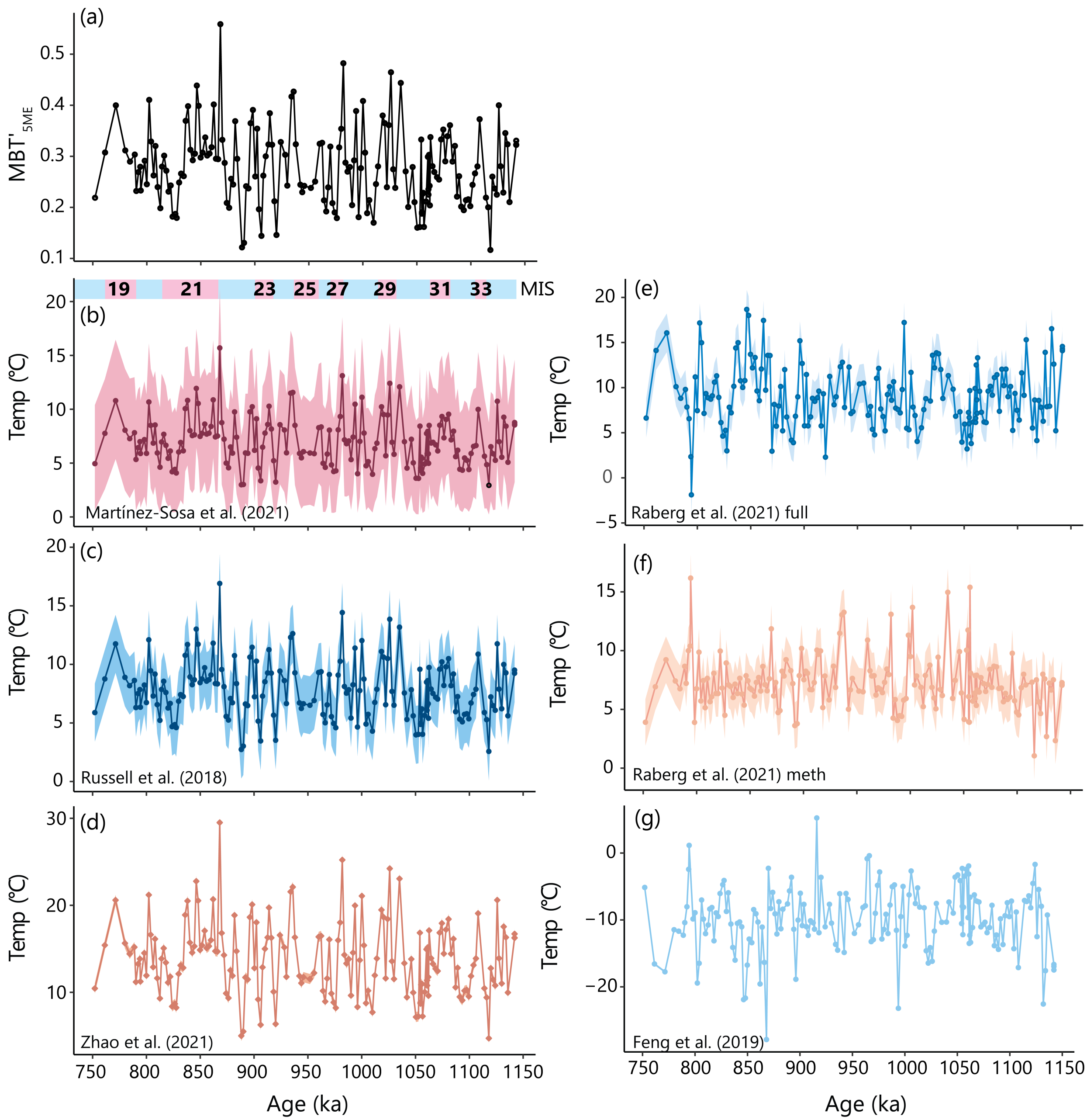

Figure S8: Application and comparison of different lacustrine-based calibrations for the Lake El'gygytgyn brGDGT temperature reconstruction. A) MBT′$_{5ME}$ results. B) Temperature of the months above freezing, based on the BayMBT calibration (Martínez-Sosa et al., 2021). C) Mean annual air temperature based on the African lakes calibration (Russell et al., 2018). D) Integrated water column temperature based on the in-situ calibration in Greenland lake (Zhao et al., 2021). E and F) Temperature of months above freezing using the calibration of Raberg et al. (2021) using the "Full" brGDGT suite and the "Meth" suite, respectively. G) Mean annual temperature following the stepwise-forward selection model of Feng et al. (2019). Shaded areas represent the uncertainty associated with each calibration.

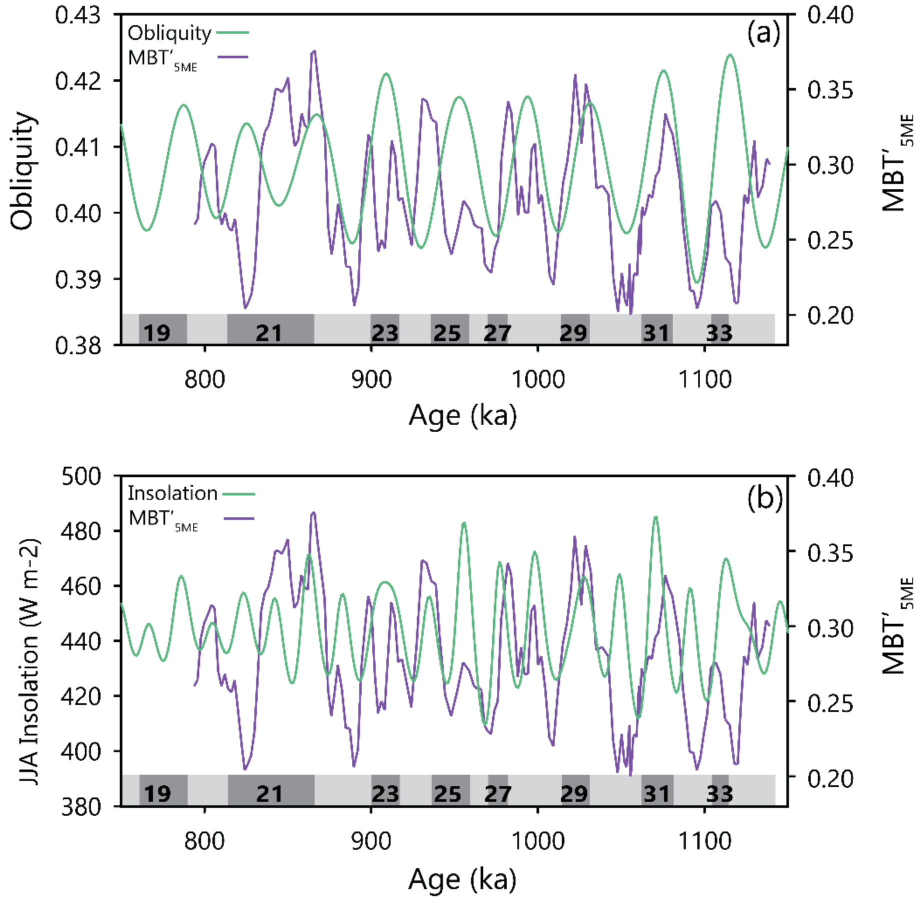

Figure S9: Comparison of the Lake El'gygytgyn brGDGT temperature reconstruction with astronomical forcings from Laskar et al. (2004). A) MBT′$_{5ME}$ results and obliquity. B) MBT′$_{5ME}$ results and insolation (June 21-Sept. 21) at 65º N latitude.

References:

Bray, E., and Evans, E.: Distribution of n-paraffins as a clue to recognition of source beds, Geochimica et Cosmochimica Acta, 22, 2-15, 1961.

Capron, E., Rasmussen, S., Popp, T., Erhardt, T., Fischer, H., Landais, A., Pedro, J., Vettoretti, G., Grinsted, A., and Gkinis, V.: The anatomy of past abrupt warmings recorded in Greenland ice, Nature communications, 12, 1-12, 2021.

Dang, X., Ding, W., Yang, H., Pancost, R. D., Naafs, B. D. A., Xue, J., Lin, X., Lu, J., and Xie, S.: Different temperature dependence of the bacterial brGDGT isomers in 35 Chinese lake sediments compared to that in soils, Organic Geochemistry, 119, 72-79, 2018.

de Wet, G. A., Castañeda, I. S., DeConto, R. M., and Brigham-Grette, J.: A high-resolution mid-Pleistocene temperature record from Arctic Lake El'gygytgyn: a 50 kyr super interglacial from MIS 33 to MIS 31?, Earth and Planetary Science Letters, 436, 56-63, 10.1016/j.epsl.2015.12.021, 2016.

Feng, X., Zhao, C., D'Andrea, W. J., Liang, J., Zhou, A., and Shen, J.: Temperature fluctuations during the Common Era in subtropical southwestern China inferred from brGDGTs in a remote alpine lake, Earth and Planetary Science Letters, 510, 26-36, 2019.

Hopmans, E. C., Schouten, S., Pancost, R. D., van der Meer, M. T., and Sinninghe Damsté, J. S.: Analysis of intact tetraether lipids in archaeal cell material and sediments by high performance liquid chromatography/atmospheric pressure chemical ionization mass spectrometry, Rapid Communications in Mass Spectrometry, 14, 585-589, 2000.

Hopmans, E. C., Schouten, S., and Sinninghe Damsté, J. S.: The effect of improved chromatography on GDGT-based palaeoproxies, Organic Geochemistry, 93, 1-6, 2016.

Kusch, S., Winterfeld, M., Mollenhauer, G., Höfle, S. T., Schirrmeister, L., Schwamborn, G., and Rethemeyer, J.: Glycerol dialkyl glycerol tetraethers (GDGTs) in high latitude Siberian permafrost: Diversity, environmental controls, and implications for proxy applications, Organic Geochemistry, 136, 103888, 2019.

Laskar, J., Robutel, P., Joutel, F., Gastineau, M., Correia, A., and Levrard, B.: A long-term numerical solution for the insolation quantities of the Earth, Astronomy & Astrophysics, 428, 261-285, 2004.

Martínez-Sosa, P., Tierney, J., Stefanescu, I. C., Crampton-Flood, E. D., Shuman, B. N., and Routson, C.: A global Bayesian temperature calibration for lacustrine brGDGTs, 2021.

Naafs, B. D. A., Inglis, G. N., Zheng, Y., Amesbury, M., Biester, H., Bindler, R., Blewett, J., Burrows, M., Del Castillo Torres, D., and Chambers, F. M.: Introducing global peat-specific temperature and pH calibrations based on brGDGT bacterial lipids, Geochimica et Cosmochimica Acta, 208, 285-301, 2017.

Raberg, J. H., Harning, D. J., Crump, S. E., de Wet, G., Blumm, A., Kopf, S., Geirsdóttir, Á., Miller, G. H., and Sepúlveda, J.: Revised fractional abundances and warm-season temperatures substantially improve brGDGT calibrations in lake sediments, Biogeosciences Discussions, 1-36, 2021.

Russell, J. M., Hopmans, E. C., Loomis, S. E., Liang, J., and Sinninghe Damsté, J. S.: Distributions of 5-and 6-methyl branched glycerol dialkyl glycerol tetraethers (brGDGTs) in East African lake sediment: Effects of temperature, pH, and new lacustrine paleotemperature calibrations, Organic Geochemistry, 117, 56-69, 2018.

Weber, Y., Damsté, J. S. S., Zopfi, J., De Jonge, C., Gilli, A., Schubert, C. J., Lepori, F., Lehmann, M. F., and Niemann, H.: Redox-dependent niche differentiation provides evidence for multiple bacterial sources of glycerol tetraether lipids in lakes, Proceedings of the National Academy of Sciences, 115, 10926-10931, 2018.

Weijers, J. W., Schouten, S., van den Donker, J. C., Hopmans, E. C., and Sinninghe Damsté, J. S.: Environmental controls on bacterial tetraether membrane lipid distribution in soils, Geochimica et Cosmochimica Acta, 71, 703-713, 2007.

Zhao, B., Castañeda, I. S., Bradley, R. S., Salacup, J. M., Gregory, A., Daniels, W. C., and Schneider, T.: Development of an in situ branched GDGT calibration in Lake 578, southern Greenland, Organic Geochemistry, 104168, 2021.

Zhao, W., Tarasov, P. E., Lozhkin, A. V., Anderson, P. M., Andreev, A. A., Korzun, J. A., Melles, M., Nedorubova, E. Y., and Wennrich, V.: High-latitude vegetation and climate changes during the Mid-Pleistocene Transition inferred from a palynological record from Lake El'gygytgyn, NE Russian Arctic, Boreas, 47, 137-149, 2018.